

## Production of Silver Nanoparticles Mediated by Aqueous Extracts of Tucumã (*Astrocaryum aculeatum*) Pulp

Sidney S. dos Santos,<sup>1b</sup> Ricardo A. A. de Couto,<sup>b</sup> Ingrid R. da Silva,<sup>c</sup> Marcia Regina M. Aouada,<sup>d</sup> Vera R. L. Costantino,<sup>1b</sup> Luiz P. da Costa<sup>1b, a, e</sup> and Gustavo F. Perotti<sup>1b, \*, a</sup>

<sup>a</sup>Instituto de Ciências Exatas e Tecnologia, Universidade Federal do Amazonas (UFAM),  
Rua Nossa Senhora do Rosário, 3863, 69103-128 Itacoatiara-AM, Brazil

<sup>b</sup>Departamento de Química Fundamental, Instituto de Química, Universidade de São Paulo (USP),  
Avenida Prof. Lineu Prestes, 748, 05508-000 São Paulo-SP, Brazil

<sup>c</sup>Centro de Biotecnologia da Amazônia (CBA), Avenida Governador Danilo de Matos Areosa, 690,  
69075-351 Manaus-AM, Brazil

<sup>d</sup>Departamento de Física e Química, Universidade Estadual Paulista (UNESP), Avenida Brasil, 56,  
15385-000 Ilha Solteira-SP, Brazil

<sup>e</sup>Departamento de Química, Universidade Federal de Sergipe (UFS), Avenida Marechal Rondon, s/n,  
49100-000 São Cristóvão-SE, Brazil

Tucumã (*Astrocaryum aculeatum*) pulp presents a large number of secondary metabolites that can mediate the synthesis of metallic nanoparticles through a greener and more sustainable synthetic route than traditional ones. This study investigated the production of silver nanoparticles (AgNPs) mediated by aqueous extracts of tucumã pulp assessing different parameters, such as temperature, concentration of extract, and pH values of the reaction media. The alkaline reaction media produced the most intense and well-defined bands around 400 nm in the electronic spectra, indicating the formation of AgNPs in the three concentrations of tucumã pulp evaluated. The increase in the temperature of the reaction media also enhanced the surface plasmon resonance band of AgNPs but it increased the polydispersivity of produced nanoparticles according to the dynamic light scattering (DLS) and transmission electron microscopy (TEM) data. Zeta potential results indicated moderate stability of the AgNPs (close to -30 mV). Antimicrobial assessment of the colloidal metal particles indicated microbicide activity against the Gram-negative *Escherichia coli* bacterium.

**Keywords:** green synthesis, alternative routes, plant extract, Amazonian resources

### Introduction

Metal nanoparticles have been extensively investigated owing to their enhanced physical and chemical properties in comparison to micro/macro-scale metal structures.<sup>1,2</sup> These properties are not solely related to the size of these nanoparticles (1 to 100 nm) but also to their shape and to the presence of other compounds on their surface.<sup>3,4</sup>

In comparison to other noble metals, silver has appealed to nanoscience researchers owing to its lower cost, low toxicity to humans, and high chemical and colloidal stability.<sup>5-7</sup> Furthermore, the formation of colloidal

silver nanoparticles can be easily monitored by low-cost techniques, such as UV-Vis spectroscopy, which allows the visualization of the surface plasmon resonance (SPR) band within the visible range.<sup>8</sup> The improved physical and chemical properties of silver nanoparticles (AgNPs) have wide applications, e.g., electronics, water treatment, catalysis, therapies, and microbial systems.<sup>9-11</sup>

One of the main concerns regarding the traditional synthesis of AgNPs is the potential toxicity of the precursors used in it or its byproducts after the reduction of silver ions, e.g., sodium borohydride, *N,N*-dimethylformamide (DMF), and hydrazine (N<sub>2</sub>H<sub>2</sub>).<sup>12</sup> Also, the reaction medium often requires another compound to control and stabilize the dispersed nanoparticles.<sup>13</sup> These issues may not only limit the range of applications of such nanostructures but

\*e-mail: gustavoperotti@ufam.edu.br

Editor handled this article: Izaura C. N. Diógenes (Associate)

also raise concerns about potential environmental impacts caused by extensive use. Hence, new strategies to overcome these disadvantages are of great importance.

In line with the adoption of sustainable technologies, the green synthesis of AgNPs was proposed in the early 2000s, using different plant parts and sources of extracts.<sup>14</sup> According to this approach, the secondary metabolites present in these extracts can reduce transition metal ions and stabilize the colloidal metal nanoparticle system in water by adhering to the surface of these nanostructures.<sup>15</sup>

In this context, the Amazonian biome, with the highest biodiversity in the world,<sup>16</sup> provides a rich trove of renewable chemical products to mediate the production of nanoparticles. The use of plant-based technology can be an effective way to increase the importance of policies for economic growth concomitant to conservation of native forests. Native to Central and South America, tucumã (*Astrocaryum aculeatum*) is a common palm tree. In Brazil, it is present from the southeast area of the Amazon Basin all the way to the west, to the States of Goiás and Mato Grosso.<sup>17</sup> Owing to its unique flavor and nutritional value, the fruit of this palm tree is consumed both *in natura* and as part of regional dishes.<sup>18</sup> Its fibrous and orange-colored pulp is particularly caloric as it contains large amounts of fatty acids, especially unsaturated ones, as well as a wide variety of other secondary metabolites, e.g., phenolic compounds and carotenoids.<sup>19,20</sup> Currently, the fruit exhibits low technological exploration and no studies are reported about the uses of its pulp extract for the synthesis of metallic nanomaterials.

Although the secondary metabolites content of tucumã can be significantly affected by weather and ontogenetic conditions related to its cultivation, its pulp has significant content of phenolic compounds such as gallic acid, rutin, quercetin, and catechin, besides beta-carotene (provitamin A), and ascorbic acid, thereby providing its aqueous pulp extract a high antioxidant capacity.<sup>20,21</sup>

For all reasons mentioned in this introduction, the present study evaluated the mediation capacity of aqueous extracts of tucumã pulp for the production of colloidal AgNPs dispersions, investigating the experimental parameters that affect the formation of these nanostructures such as concentration of the aqueous tucumã pulp extract, pH, temperature, and reaction time. The antimicrobial properties of the obtained dispersions were also investigated.

## Experimental

Nitric acid P.A. (HNO<sub>3</sub>, Vetec, Duque de Caxias, Brazil), sodium hydroxide P.A. (NaOH, Labsynth, Diadema,

Brazil), silver nitrate P.A. (AgNO<sub>3</sub>, Laderquímica, Vitória, Brazil), Luria Bertani (LB) broth and Mueller-Hinton agar (Kasvi, São José do Pinhais, Brazil) were used without further purification. All solutions were prepared with distilled water.

### Preparation of aqueous extracts of tucumã pulp

After peeling of fruit and disposing of seeds, different amounts of tucumã pulp (1.0, 1.5, and 2.0 g) were weighed (Shimadzu analytical scale model AU220, Kyoto, Japan) and later macerated with pestle and mortar in 50 mL of distilled water for 5 min, transferred to another container with 50 mL of distilled water, and left to rest in refrigeration at 4 °C for 24 h. Then, their liquid fractions were collected by centrifugation (Centrifuge model 80-20, Shanghai, China) at 4,000 rpm for 10 min and used within one week after preparation and stored under refrigeration. These pulp extracts were labeled as follows: C1 (1.0 g of pulp in 100 mL of distilled water), C2 (1.5 g of pulp in 100 mL of distilled water), and C3 (2.0 g of pulp in 100 mL of distilled water).

### Production of colloidal dispersions of silver nanoparticles

The reaction media for producing AgNPs consisted of 5 mL of tucumã pulp at different concentrations and 50 mL of silver nitrate solution (0.01 mmol L<sup>-1</sup>) resulting in a total volume of 55 mL in each vessel. After mixing, the pH value of each reaction medium was adjusted to 5.0, 7.0, and 9.0 (Hanna pHmeter model HI8424, Woonsocket, USA) with sodium hydroxide or nitric acid solutions (0.05 mmol L<sup>-1</sup>). Each vessel was wrapped in aluminum foil and kept under constant agitation (Cienlab magnetic stirrer model CE-1540/A, Campinas, Brazil) at 30 °C for 24 h. Then, the reaction vessels were left undisturbed at room temperature for the remainder of the experiments. Other temperature values (40 and 50 °C) were also assessed and followed the same procedure aforementioned above for 24 h.

### Antimicrobial activity of obtained AgNPs

Microbiological tests were conducted using the Gram-negative bacteria *Escherichia coli* (ATCC 25992) and *Streptococcus pneumoniae* (ATCC 49619), Gram-positive bacteria *Staphylococcus aureus* (ATCC 25923) and *Klebsiella pneumoniae* (ATCC 700603), and *Candida albicans* (ATCC 10231) yeast by agar diffusion in order to determine inhibition zones. Prior to analysis, the materials were sterilized in an autoclave at 121 °C for 20 min.

The bacteria and yeast were initially cultured for 24 h before inoculation in Luria Bertani nutritive broth (LB). The agar medium was prepared using 36 g of Muller-Hinton agar in 1.0 L of distilled water. Approximately 50 mL of this medium were transferred to Petri dishes and left to rest at 37 °C in a laboratory oven. After drying, a glass tube was employed to create five wells in each Petri dish, to which the test liquids were added.

The bacterial cultures were diluted with saline solution (0.85% (m/m) NaCl) to the absorbance value of 0.03 at 600 nm, and transferred to the Petri dishes using sterile swabs. Then, 100 µL of the solutions and dispersions, prepared without further dilution, were transferred to the wells and left to rest at 37 °C for 24 h in a laboratory oven before analysis of inhibition zones. All tests were performed in triplicate. The C2 tucumã extract was used to produce all of the tested AgNPs dispersions and were labeled as sample 1 (produced at pH 9.0 and 30 °C), 2 (pH 7.0; 40 °C), 3 (pH 9.0; 40 °C), 4 (pH 7.0; 50 °C), 5 (pH 9.0; 50 °C), 6 (C2 tucumã extract), and 7 (0.01 mmol L<sup>-1</sup> silver nitrate solution). Solutions of amoxicillin and fluconazole at 50 mg mL<sup>-1</sup> were used as positive control for bacteria and yeast, respectively, in these experiments. The obtained inhibition halo values were expressed as arithmetic mean ± standard deviation.

#### Characterization techniques

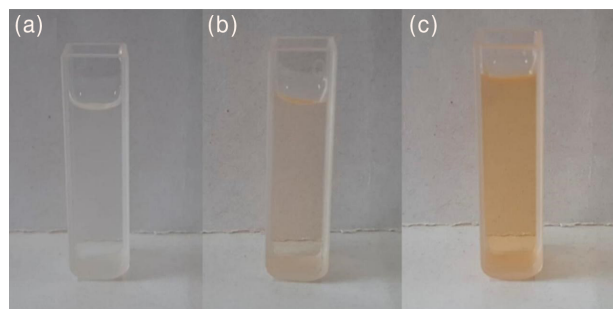
UV-Vis analysis was performed on a Bel equipment (UV-M51, Monza, Italy) using distilled water as blank and spectral region between 180-750 nm to investigate the surface plasmon resonance band of AgNPs present in each media. After mixing the pulp extracts and silver nitrate solutions and adjusting the pH value, the media were analyzed every 10 min for the first hour, every hour for up to 4 h, every 12 h for the first 2 days, and every 24 h for 21 days. The aqueous tucumã extract also had its spectrum recorded after performing a 1:20 dilution (C2 extract:distilled water).

The analysis of the hydrodynamic diameter and the zeta potential of the produced dispersions were performed on a Malvern Pananalytical equipment (Zetasizer NanoZS, Malvern, UK) using a helium-neon laser (4 mW) operating at 633 nm wavelength and angle of collection of the light beam at 173°. Prior to readings, the samples were diluted with deionized water. Three replicates of each sample were performed in automatic mode at 25 °C. Zeta potentials were measured in manual mode three times using a capillary electrophoresis cell (DTS-1070, Malvern, UK). The obtained values from dynamic light scattering (DLS) and zeta potential measurements were expressed as arithmetic mean ± standard deviation.

The transmission electron microscopy (TEM) images and X-ray spectroscopy (EDS) analysis were recorded on a Tecnai G<sup>2</sup> F20 microscope (Hillsboro, USA). The samples were prepared by the drop-casting approach, where AgNPs dispersions were diluted in deionized water and later deposited on a carbon-coated copper grid, followed by room temperature drying for 1 h.

## Results and Discussion

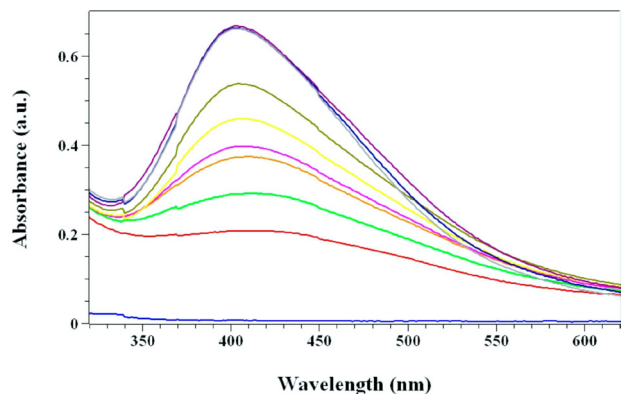
After mixing the solution containing the silver precursor salt and the aqueous tucumã extract at different concentrations, a color change was observed in the reaction media, from clear to light brown and increasingly darker as the reaction progressed, as shown in Figure 1. This change derives from the interaction of the AgNPs with light, resulting in a collective oscillation of the conduction band electrons of these metallic atoms, a phenomenon known as SPR.<sup>22</sup> This brownish hue is typical of AgNPs dispersions<sup>23-25</sup> and its increasing intensity is attributed to higher concentrations of nanoparticles in the reaction medium, according to the Beer-Lambert Law.<sup>2,26</sup>



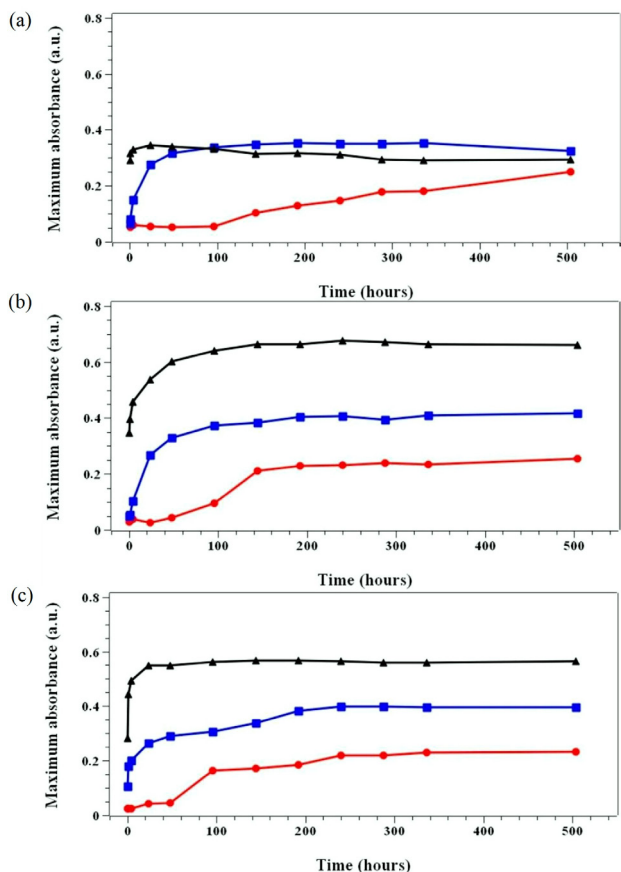
**Figure 1.** Images of the reaction medium containing the silver precursor salt and the aqueous tucumã extract (C2) at different stages: (a) after 5 min, (b) after 3 h, and (c) after 3 days of reaction.

Figure 2 shows the UV-Vis electronic spectra of the tucumã extract and the tucumã extract mixed with the silver nitrate solution as a function of reaction time using the C2 extract and pH 9.0. The band exhibits maximum absorbance close to 400 nm related to the SPR band of the formed AgNPs.<sup>3,27</sup> It is also observed the progressive increase in absorbance of this band during the 21-day reaction time, indicating that the formation of AgNPs is slow under the experimental conditions used in this study.

Figure 3 shows the evolution of the maximum absorbance value of the SPR band for the reaction media with different plant extract concentrations and at different pH values and 30 °C. All plant extract conditions in alkaline reaction media resulted in formation of larger amounts of AgNPs in a shorter time (about 24 h) compared to the synthesis performed at pH 5.0 or 7.0. The results obtained



**Figure 2.** UV-Vis spectra of the reaction medium using the tucumã extract C2 (1.5 g of pulp in 100 mL of water, blue line) at pH 9.0 and temperature of 30 °C after 10 min (red), 20 min (light green), 40 min (orange), 1 h (purple), 4 h (yellow), 1 day (dark green), 7 days (dark blue), 14 days (purple), and 21 days (gray) of reaction.



**Figure 3.** Evolution of maximum absorbance values related to SPR bands of dispersions of AgNPs obtained at pH 5.0 (red), pH 7.0 (blue), and pH 9.0 (black) using 1.0 g C1 (a), 1.5 g C2 (b), and 2.0 g C3 (c) of tucumã pulp in 100 mL of water.

for the maximum absorbance of the SPR band in the three conditions of plant extract concentration at pH 5.0 were similar (approximately 0.25) and exhibited slower band evolution and lower intensity in comparison to other pH values. These results suggest that the presence of few previously silver atoms (seeds for the growth of AgNPs,

also known as the nucleation stage) boosts the growth of the formed nanostructures, rendering them larger and more polydisperse among themselves.<sup>28,29</sup>

The concentration of plant extract affects the rate of formation of AgNPs and the total amount of nanoparticles formed. Hence, high tucumã concentrations in the reaction medium (C2 and C3; Figures 3b and 3c) resulted in more intense SPR bands and in a shorter time as compared to those of C1 at the same pH values.

Specifically for C1, Figure 3a shows a decrease in maximum absorbance associated with the SPR bands of AgNPs at pH 7.0 and 9.0 as compared to pH 5.0. Under C1, since pH 9.0 generated a larger formation of AgNPs in a short time and there were lower amounts of secondary metabolites in the reaction medium to bind to the surface of the formed nanoparticles, the colloidal system displayed reduced stability, e.g., the nanoparticles aggregated after some time. Similar trends were found by Jain and Mehata<sup>24</sup> using low concentrations of plant extract from *Ocimum sanctum* leaves (Tulsi). On the other hand, an intensity decrease in maximum absorbance for longer reaction periods may also occur owing to the adsorption of AgNPs over the glass wall of each reaction vessel.<sup>30</sup>

Figure 4 shows the absorbance values of the SPR band of the reaction media using the C2 plant extract at pH 9.0 and temperature values of 30, 40, and 50 °C. The results suggest that temperature has a direct influence on the formation of the AgNPs. This is possibly related to the increase in kinetic energy of the reactant species (ions and molecules) promoted by temperature and, consequently, a higher probability that collisions among reactants overcome the potential barrier, leading to product formation.<sup>31,32</sup> After reaching the maximum absorbance for the SPR band, there was a decrease in the pH of the reaction media from 9.0 to 7.82 for the sample at 30 °C, to 7.55 at 40 °C and to 7.42 at 50 °C, suggesting the rupture of O–H bonds in different

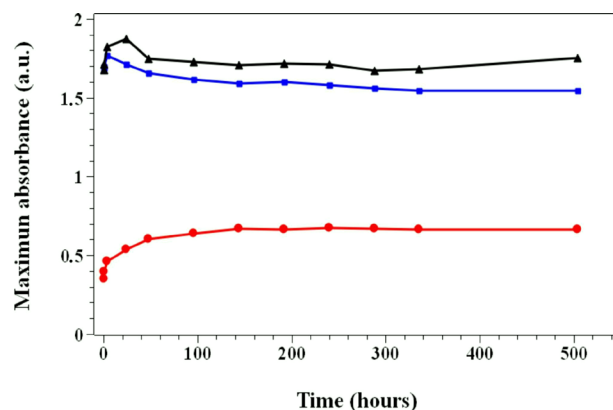


**Figure 4.** Evolution of maximum absorbance value related to the SPR band for the C2 reaction media (1.5 g of pulp in 100 mL water) at pH 9.0 and 30 °C (red), 40 °C (blue), and 50 °C (black).

secondary metabolites with antioxidant properties, such as the phenolic compounds found in the pulp of tucumã,<sup>19,20</sup> decreasing the alkalinity of the colloids through the release of H<sup>+</sup> ions. The rupture of this bond is believed to be the first of several reactions involved in the reduction mechanism of silver ions.<sup>33,34</sup> Another feature was observed in the sample at produced 40 °C, the only medium that reached the maximum absorbance value of the SPR band close to 4 h of reaction.

The results suggest that increasing the temperature results in higher capacity of the tucumã plant extract to reduce silver instead of degrading the biomolecules involved in this step. Hence, the crossing of the potential barrier is more frequent from the beginning of the reaction, resulting in a higher product formation rate in a shorter time. In brief, an increase in temperature accelerates AgNPs nucleation and stabilization steps. In the case of plant extracts, as temperature increases, there is higher conversion of the reducing agent to an oxidized product, consequently increasing the release of electrons to the silver(I) cations. As this is an important step in AgNPs synthesis, it can be optimized at high temperatures.<sup>28,31,32</sup>

Figure 5 shows the hydrodynamic diameter distribution for AgNPs obtained by DLS technique using the C2 tucumã extract (1.5 g of pulp in 100 mL of water) in alkaline medium (pH 9.0) at three temperature values (30, 40, and 50 °C). The observed average hydrodynamic diameters were 23.5 ± 1.2 nm (30 °C), 18.8 ± 1.0 nm (40 °C), and 32.0 ± 2.2 nm (50 °C).

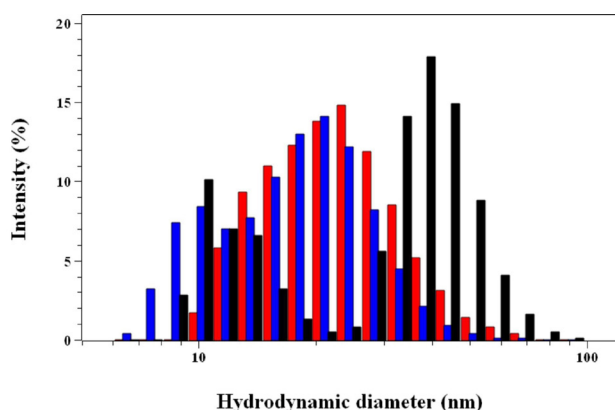


**Figure 5.** Average hydrodynamic diameters observed for C2 samples (1.5 g of pulp in 100 mL of water) at pH 9.0 and 30 °C (red), 40 °C (blue), and 50 °C (black) after 21 days of reaction.

The AgNPs produced at 40 and 50 °C display a bimodal distribution, with one of higher intensity and a second of lower intensity, as shown in Figure 5. It is noticed that the sample obtained at 40 °C exhibits a higher tendency to form AgNPs of smaller diameter as it also exhibits the smallest average size among the samples under investigation. This

may be a result of the AgNPs formation rate under this condition, as aforementioned, since it was the sole sample to reach maximum absorbance within 4 h of reaction time.

DLS results suggest that an increase in temperature (40 °C) promotes the formation of AgNPs with smaller average hydrodynamic diameter. As the temperature value further increases (50 °C), polydispersity, e.g., AgNPs populations of differing particle sizes are formed. This indicates that temperature values above 40 °C hinder stabilization of silver nanostructures, promoting their aggregation and formation of more polydisperse populations with respect to hydrodynamic diameter. A probable explanation for this phenomenon is the thermal degradation of some types of biomolecules responsible for stabilizing these nanoparticles, e.g., phenolic compounds, as reported by Inns *et al.*,<sup>35</sup> who exposed this class of compounds to temperature values above 50 °C.

The polydispersity index (PDI) is also a parameter used to measure nanoparticle size and distribution. In the PDI, the value varies from 0 to 1; the closer to 0, the more monodisperse the system under analysis is, e.g., the more homogeneous the AgNPs are. Within this frame of reference, the PDI values obtained for the samples were 0.375 (30 °C), 0.356 (40 °C), and 0.465 (50 °C), indicating the existence of wide variation in the NPs obtained in this study. According to Bonatto and Silva,<sup>36</sup> AgNPs synthesis mediated by plant extracts usually exhibit moderate PDI values, e.g., from 0.3 to 0.5. Other studies also showed similar range of PDI values when using different plant extracts, such as *Citrus limon* and *Nigella sativa*.<sup>37,38</sup>

The samples produced in the present study exhibited average surface charges of  $-28.6 \pm 1.3$  (30 °C),  $-28.4 \pm 0.2$  (40 °C), and  $-27.4 \pm 0.4$  (50 °C) mV. As stated by Clogston and Patri,<sup>39</sup> particles with high zeta potential and the same sign of charge, whether positive ( $> +30$  mV) or negative ( $< -30$  mV), will repel each other. Hence, in spite of their zeta potential being close to  $-30$  mV, the samples exhibit a moderate tendency to aggregate. The zeta potential data corroborated the results obtained during the experiments at the laboratory. After the samples reached the maximum absorbance value, AgNPs deposition could be observed over time. The AgNPs samples produced at high temperature formed low amounts of sediments after the first reaction day, especially the ones at pH 7.0. On the other hand, the samples produced at 30 °C precipitated after 5 days from the start of the reaction. These negative values might be associated with the presence of carboxylate groups present in the structure of the biomolecules responsible for AgNPs stabilization.

The TEM images of the AgNPs particles synthesized using the C2 tucumã extract and reaction media at pH 9.0 and temperatures of 30 and 40 °C are presented in Figure 6.

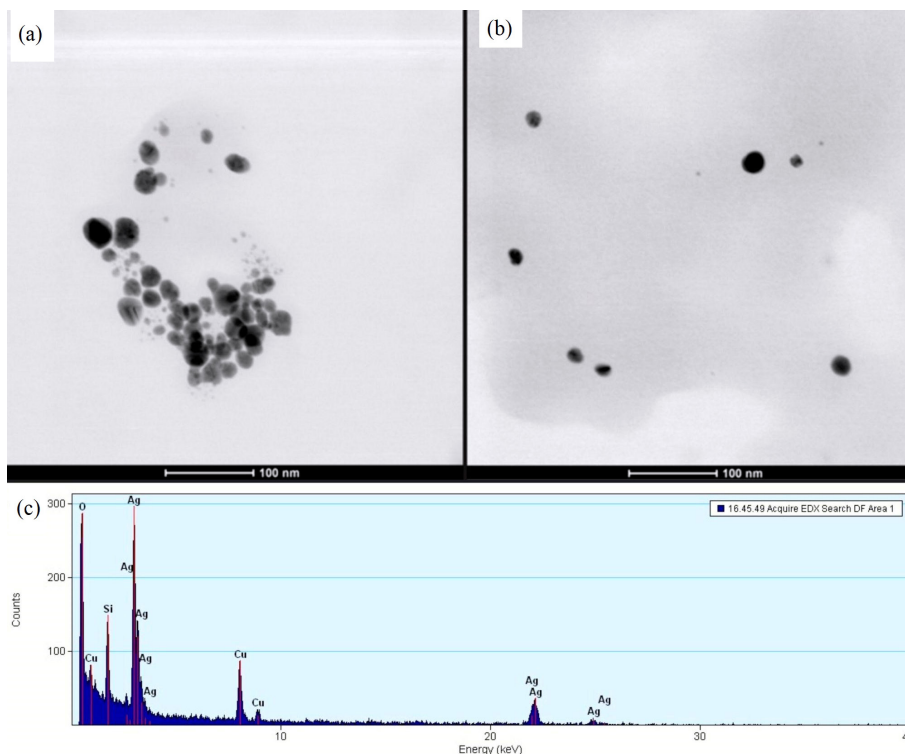


**Figure 6.** Transmission electron microscopy (TEM) images of AgNPs using the C2 tucumã extract (1.5 g of pulp in 100 mL of water) at pH 9.0 and temperature of (a) 30 °C and (b) 40 °C after 14 days of reaction. Energy dispersive spectroscopy (EDS) data of the (a) image (c).

The nanoparticles presented predominantly spheroidal morphology, whereas the sample obtained at 30 °C exhibited dimensions around 30 nm, while at 40 °C formed nanostructures closer to 20 nm. These results corroborate the DLS data, demonstrating the effect of temperature on the reaction speed and average size of these AgNPs, as aforementioned. Additionally, the EDS data confirmed that these structures are formed by silver atoms.

Figure 7 shows the results of microbiological tests by the agar diffusion technique; antimicrobial activity was detected for samples 3 and 7 against *Escherichia coli*, both with  $1.2 \pm 0.1$  cm halo. The tested AgNPs dispersions only exhibited antimicrobial activity against *Escherichia coli*, which is a susceptible bacterium to the microbicide effect of AgNPs.<sup>40-42</sup> This phenomenon may be explained in two ways: it may be owing to Gram-positive bacteria having thicker cell walls (as a result of having a higher amount of peptidoglycan as compared to Gram-negative bacteria) and/or to the presence of lipoteichoic acid in Gram-positive bacteria, increasing their protection against external agents.<sup>43,44</sup>

Some authors<sup>41,45,46</sup> attribute the antibacterial effect to the size of AgNPs, e.g., the smaller their diameter, the more effective they are against microorganisms due to easier penetration in their cells. Accordingly, the AgNPs synthesis in an alkaline medium with moderate concentration of plant extract at 40 °C (Table 1), which produced nanoparticles with smaller diameters ( $18.8 \pm 1.0$  nm) as

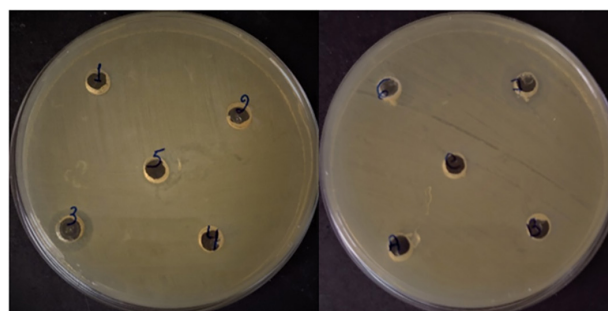


**Figure 7.** Antibigram of *Escherichia coli* evidencing inhibition halos for samples 3 (AgNPs formed using C2 tucumã pulp extract and synthesis at pH 9.0 and 40 °C-bottom left well on the left image) and 7 (0.01 mol L<sup>-1</sup> silver nitrate solution-top right well on the right image).

compared to the other conditions under investigation, provided the most effective antimicrobial activity.

Some authors<sup>45,46</sup> suggest that the overall surface area of AgNPs in a system is directly related to their bactericidal activity. When the average size of these nanostructures is reduced, the overall surface area increases, enhancing the antimicrobial response due to higher interaction with existing bacteria. That is, the antibacterial potential of AgNPs is amplified by increasing their overall surface area, which promotes the release of a higher number of Ag<sup>+</sup> cations. These ionic species then bind to negatively charged functional groups of molecules present in bacterial cell walls, leading to disruption, enzyme deactivation and/or changes in membrane permeability.<sup>47,48</sup>

**Table 1.** Average hydrodynamic diameter of AgNPs as a function of pH and temperature

pH	9.0	7.0	9.0	7.0	9.0
Temperature / °C	30	40	40	50	50
Average diameter / nm	23.5	77.0	18.8	74.8	32.0
Standard deviation	1.2	3.8	1.0	3.2	2.2

## Conclusions

The results obtained in this study not only indicate the involvement of secondary metabolites in the reduction reaction of silver(I) ions, but also that their concentration influences the stability and amount of AgNPs formed. Temperature and pH also affect the formation of AgNPs and their stabilization.

UV-Vis spectroscopy results, corroborated by DLS, TEM and microbiological test results, demonstrated that the dispersion formed using 1.5 g of tucumã pulp in 100 mL water (C2) at pH 9.0 and the temperature of 40 °C were the most promising conditions for producing a significant amount of nanostructures. It also showed that this was the only condition to reach maximum absorbance associated with the SPR band of the AgNPs within 4 h of reaction time, whereas for other conditions these values were registered after 24 h of reaction. DLS and TEM results indicated that the aforementioned condition produced the smallest average hydrodynamic diameter compared to the others investigated. In addition, it was the only condition to display inhibitory activity against the Gram-negative bacterium *Escherichia coli*.

## Acknowledgments

The authors are grateful to CAPES (Higher Education Personnel Improvement Coordination) for the financial support to PPCTRA-UFAM (Postgraduate Program in Science and Technology for Amazonian Resources), to CNPq (National Council for Scientific Development; grant process No. 404810/2021-7), to FAPEAM (Amazonas State Research Support Foundation; grant processes No. 062.00875/2020 and 01.02.016301.03332/2021-12 (G.F.P.), and No. 062.00876/2020 (L.P.C.)), and to FAPESP (São Paulo State Research Support Foundation; grant process No. 2011/50318 (V.R.L.C.) and 06170-1/2019 (M.R.M.A.)) for the financial support of this research. S. S. Santos is grateful for the master's scholarship granted by FAPEAM (POSGRAD 2020/2021). The authors acknowledge the Laboratory of Structural Characterization (LCE/DEMa/UFSCar) for the infrastructure support.

## Author Contributions

S. S. S. produced the tucumã extracts, prepared the AgNPs dispersion, performed UV-Vis characterization and wrote the paper; R. A. A. C. and V. R. L. C. conducted the analysis and interpretation of DLS and zeta potential data; M. R. M. A. conducted the analysis and interpretation of TEM and EDS; I. R. S. conducted the analysis and interpretation of the antimicrobial assays; L. P. C. and G. F. P. analyzed and interpreted characterization data, headed the investigation, elaborated the experimental scheme and wrote the paper. All authors revised the manuscript.

## References

- Beyene, H. D.; Werkneh, A. A.; Bezabh, H. K.; Ambaye, T. G.; *Sustainable Mater. Technol.* **2017**, *13*, 18. [Crossref]
- Erci, F.; Cakir-Koc, R.; Isildak, I.; *Artif. Cells, Nanomed., Biotechnol.* **2018**, *46*, 150. [Crossref]
- Pirtarighat, S.; Ghannadnia, M.; Baghshahi, S.; *J. Nanostruct. Chem.* **2019**, *9*, 1. [Crossref]
- Rasheed, T.; Bilal, M.; Li, C.; Nabeel, F.; Khalid, M.; Iqbal, H. M. N.; *J. Photochem. Photobiol., B* **2018**, *181*, 44. [Crossref]
- Desireddy, A.; Conn, B. E.; Guo, J.; Yoon, B.; Barnett, R. N.; Monahan, B. M.; Kirschbaum, K.; Griffith, W. P.; Whetten, R. L.; Landman, U.; Bigioni, T. P.; *Nature* **2013**, *501*, 399. [Crossref]
- Hadrup, N.; Sharma, A. K.; Loeschner, K.; *Regul. Toxicol. Pharmacol.* **2018**, *98*, 257. [Crossref]
- Schubert J.; Chanana, M.; *Curr. Med. Chem.* **2019**, *25*, 4553. [Crossref]
- Muthusamy, G.; Thangasamy, S.; Raja, M.; Chinnappan, S.; Kandasamy, S.; *Environ. Sci. Pollut. Res.* **2017**, *24*, 19459. [Crossref]
- Sherin, L.; Sohail, A.; Amjad, U. S.; Mustafa, M.; Jabeen, R.; Ul-Hamid, A.; *Colloid Interface Sci. Commun.* **2020**, *37*, 100276. [Crossref]
- Wumaier, M.; Yao, T.-M.; Hu, X.-C.; Hu, Z.-A.; Shi, S.; *Dalton Trans.* **2019**, *48*, 10393. [Crossref]
- Zhang, L.; Lu, H.; Chu, J.; Ma, J.; Fan, Y.; Wang, Z.; Ni, Y.; *ACS Sustainable Chem. Eng.* **2020**, *8*, 12655. [Crossref]
- Tarannum, N.; Divya; Gautam, Y. K.; *RSC Adv.* **2019**, *9*, 34926. [Crossref]
- Yaqoob, A. A.; Umar, K.; Ibrahim, M. N. M.; *Appl. Nanosci.* **2020**, *10*, 1369. [Crossref]
- Shankar, S. S.; Ahmad, A.; Sastry, M.; *Chem. Mater.* **2005**, *17*, 566. [Crossref]
- Ahmad, S.; Munir, S.; Zeb, N.; Ullah, A.; Khan, B.; Ali, J.; Bilal, M.; Omer, M.; Alamzeb, M. Salman, S. M.; Ali, S.; *Int. J. Nanomed.* **2019**, *14*, 50. [Crossref]
- Zabaniotou, A.; Syrgiannis, C.; Gasperin, D.; Guevera, A. J. H.; Fazenda, I.; Huisingsh, D.; *Sustainability* **2020**, *12*, 8407. [Crossref]

17. Umpierres, C. S.; Thue, P. S.; Lima, E. C.; dos Reis, G. S.; de Brum, I. A. S.; de Alencar, W. S.; Dias, S. L. P.; Dotto, G. L.; *Environ. Technol.* **2018**, *39*, 1173. [Crossref]
18. Mendonça, I. M.; Paes, O. A. R. L.; Maia, P. J. S.; Souza, M. P.; Almeida, R. A.; Silva, C. C.; Duvoisin Jr., J. R. S.; de Freitas, F. A.; *Renewable Energy* **2019**, *130*, 103. [Crossref]
19. Guex, C. G.; Cassanego, G. B.; Dornelles, R. C.; Casoti, R.; Engelmann, A. M.; Somacal, S.; Maciel, R. M.; Duarte, T.; Borges, W. S.; de Andrade, C. M.; Emanuelli, T.; Danesi, C. C.; Ribeiro, E. E.; Bauermann, L. F.; *Drug Chem. Toxicol.* **2022**, *45*, 810. [Crossref]
20. Sagrillo, M. R.; Garcia, L. F. M.; de Souza Filho, O. C. S.; Duarte, M. M. M. F.; Ribeiro, E. E.; Cadoná, F. C.; da Cruz, I. B. M.; *Food Chem.* **2015**, *173*, 741. [Crossref]
21. Santos, R. C. V.; Sagrillo, M. R.; Ribeiro, E. E.; Cruz, I. B. M. In *Exotic Fruits Reference Guide*; Rodrigues, S.; Silva, E. O.; de Brito, E. S., eds.; Academic Press: London, 2018, p. 419. [Crossref]
22. Wang, M.; Li, H.; Xu, T.; Zheng, H.; Yu, M.; Li, G.; Xu, J.; Wu, J.; *Opt. Express* **2018**, *26*, 28277. [Crossref]
23. Carson, L.; Bandara, S.; Joseph, M.; Green, T.; Grady, T.; Osuji, G.; Weerasooriya, A.; Ampim, P.; Woldesenbet, S.; *Foodborne Pathog. Dis.* **2020**, *17*, 504. [Crossref]
24. Jain, S.; Mehata, M. S.; *Sci. Rep.* **2017**, *7*, 15867. [Crossref]
25. Paiva, L.; Fidalgo, T. K. S.; da Costa, L. P.; Maia, L. C.; Balan, L.; Anselme, K.; Ploux, L.; Thiré, R. M. S. M.; *J. Dent.* **2018**, *69*, 102. [Crossref]
26. Pastoriza-Santos, I.; Liz-Marzán, L. M.; *Langmuir* **1999**, *15*, 948. [Crossref]
27. Maghsoodloo, S.; Ebrahimzadeh, M. A.; Tavakoli, S.; Mohammadi, H.; Biparva, P.; Rafiei, A.; Kardan, M.; Mohammadyan, M.; Eslami, S.; *Nanomed. Res. J.* **2020**, *5*, 171. [Crossref]
28. Dada, A. O.; Adekola, F. A.; Dada, F. E.; Adelani-Akande, A. T.; Bello, M. O.; Okonkwo, C. R.; Inyinbor, A. A.; Oluyori, A. P.; Olayanju, A.; Ajanaku, K. O.; Adetunji, C. O.; *Heliyon* **2019**, *5*, E02517. [Crossref]
29. Mosaviniya, M.; Kikhavani, T.; Tanzifi, M.; Yarak, M. T.; Tajbakhsh, P.; Lajevardi, A.; *Colloid Interface Sci. Commun.* **2019**, *33*, 100121. [Crossref]
30. da Costa, L. P.; Formiga, A. L. B.; Mazali, I. O.; Sigoli, F. A.; *Synth. Met.* **2011**, *161*, 1517. [Crossref]
31. Hamed, S.; Ghaseminezhad, M.; Shokrollahzadeh, S.; Shojaosadati, S. A.; *Artif. Cells, Nanomed., Biotechnol.* **2017**, *45*, 1588. [Crossref]
32. Liu, H.; Zhang, H.; Wang, J.; Wei, J.; *Arabian J. Chem.* **2020**, *13*, 1011. [Crossref]
33. Rao, K. J.; Paria, S.; *Mater. Res. Bull.* **2013**, *48*, 628. [Crossref]
34. Meva, F. E.; Mbeng, J. O. A.; Ebongue, C. O.; Schusenner, C.; Kokçam-Demir, U.; Ntomba, A. A.; Kedi, P. B. E.; Elanga, E.; Loudang, E. N.; Nko'o, M. H. J.; Tchoumbi, E.; Deli, V.; Nanga, C. C.; Mpondo, E. A. M.; Janiak, C.; *J. Biomater. Nanobiotechnol.* **2019**, *10*, 102. [Crossref]
35. Inns, E. L.; Buggey, L. A.; Booer, C.; Nursten, H. E.; Ames, J. M.; *J. Agric. Food Chem.* **2011**, *59*, 9335. [Crossref]
36. Bonatto, C. C.; Silva, L. P.; *Ind. Crops Prod.* **2014**, *58*, 46. [Crossref]
37. Alkhulaifi, M. M.; Alswahaibi, J. H.; Alwehaibi, M. A.; Awad, M. A.; Al-Enazi, N. M.; Aldosari, N. S.; Hatamleh, A. A.; Abdel-Raouf, N.; *Saudi J. Biol. Sci.* **2020**, *27*, 3434. [Crossref]
38. Chand, K.; Jiao, C.; Lakhan, M. N.; Shah, A. H.; Kumar, V.; Fouad, D. E.; Chandio, M. B.; Maitlo, A. A.; Ahmed, M.; Cao, D.; *Chem. Phys. Lett.* **2021**, *763*, 138218. [Crossref]
39. Clogston, J. D.; Patri, A. K. In *Characterization of Nanoparticles Intended for Drug Delivery*; McNeil, S. E., ed.; Humana Press: New York, 2011, p. 63. [Crossref]
40. Clébis, V. H.; Proni, E.; Sorimento, J. J. P.; Takayama, R. K.; Nakazato, G.; *Braz. J. Anim. Env. Res.* **2021**, *4*, 933. [Crossref]
41. Quintero-Quiroz, C.; Acevedo, N.; Zapata-Giraldo, J.; Botero, L. E.; Quintero, J.; Zárate-Trino, D.; Saldarriaga, J.; Pérez, V. Z.; *Biomater. Res.* **2019**, *23*, 27. [Crossref]
42. Ramos, M. M.; Morais, E. S.; Sena, I. S.; Lima, A. L.; de Oliveira, F. R.; de Freitas, C. M.; Fernandes, C. P.; de Carvalho, J. C. T.; Ferreira, I. M.; *Biotechnol. Lett.* **2020**, *42*, 833. [Crossref]
43. Tortora, G. J.; Funke, B. R.; Case, C. L.; *Microbiologia*, 12<sup>nd</sup> ed.; Editora Artmed: Rio de Janeiro, 2016, ch. 10.
44. Mohanbaba, S.; Gurunathan, S. In *Nanobiomaterials in Antimicrobial Therapy: Applications of Nanomaterials*; Grumezescu, A. M., ed.; William Andrew Applied Science Publishers: Bucharest, 2016, ch. 6. [Crossref]
45. Ahmed, F.; Omar, S. Y.; Albalawi, F.; Arshi, N.; Dwivedi, S.; Kumar, S.; Shaalan, N. M.; Ahmad, N.; *Crystals* **2021**, *11*, 666. [Crossref]
46. Nurul Aini, A.; Farraj, D. A.; Endarko, E.; Rubiyanto, A.; Nur, H.; Khulaifi, M. M.; Hadibarata, T.; Syafiuddin, A.; *J. Chin. Chem. Soc.* **2019**, *66*, 705. [Crossref]
47. Kalwar, K.; Shan, D.; *Micro Nano Lett.* **2018**, *13*, 277. [Crossref]
48. Koduru, J. R.; Kailasa, S. K.; Bhamore, J. R.; Kim, K.; Dutta, T.; Vellingiri, K.; *Adv. Colloid Interfacial Sci.* **2018**, *256*, 326. [Crossref]

Submitted: July 13, 2022

Published online: November 11, 2022

